Electrophysiological Changes During Early Steps of Retinitis Pigmentosa

Ulisse Bocchero,[1] Beatrice M. Tam,[2] Colette N. Chiu,[2] Vincent Torre,[1] and Orson L. Moritz[2]

[1]Neuroscience Department, International School for Advanced Studies (SISSA), Trieste, Italy
[2]Department of Ophthalmology and Visual Sciences, University of British Columbia, Vancouver, British Columbia, Canada

Correspondence: Vincent Torre, International School for Advanced Studies (SISSA), via Bonomea 265, Trieste 34136, Italy; torre@sissa.it.
Orson L. Moritz, Department of Ophthalmology and Visual Sciences, University of British Columbia, 2550 Willow Street, Vancouver, BC V5Z 3N9, Canada; olmoritz@mail.ubc.ca.

Submitted: July 23, 2018
Accepted: December 29, 2018

Citation: Bocchero U, Tam BM, Chiu CN, Torre V, Moritz OL. Electrophysiological changes during early steps of retinitis pigmentosa. *Invest Ophthalmol Vis Sci*. 2019;60:933–943. https://doi.org/10.1167/iovs.18-25347

Purpose. The rhodopsin mutation *P23H* is responsible for a significant portion of autosomal-dominant retinitis pigmentosa, a disorder characterized by rod photoreceptor death. The mechanisms of toxicity remain unclear; previous studies implicate destabilization of P23H rhodopsin during light exposure, causing decreased endoplasmic reticulum (ER) exit and ER stress responses. Here, we probed phototransduction in *Xenopus laevis* rods expressing bovine P23H rhodopsin, in which retinal degeneration is inducible by light exposure, in order to examine early physiological changes that occur during retinal degeneration.

Methods. We recorded single-cell and whole-retina responses to light stimuli using electrophysiology. Moreover, we monitored morphologic changes in rods after different periods of light exposure.

Results. Initially, *P23H* rods had almost normal photoresponses, but following a brief light exposure varying from 4 to 32 photoisomerizations per disc, photoresponses became irreversibly prolonged. In intact retinas, rods began to shed OS fragments after a rod-saturating exposure of 12 minutes, corresponding to approximately 10 to 100 times more photoisomerizations.

Conclusions. Our results indicate that in *P23H* rods light-induced degeneration occurs in at least two stages, the first involving impairment of phototransduction and the second involving initiation of morphologic changes.

Keywords: retinitis pigmentosa, phototransduction, photoresponse, rhodopsin, photoreceptor

Rod outer segments (OSs) are comprise thousands of stacked discs containing photon-absorbing rhodopsin molecules packed in an almost crystalline fashion.[1–5] Photo-excited rhodopsins activate G-proteins, each of which activates one phosphodiesterase (PDE) molecule.[6–8] Activated PDEs hydrolyze cyclic guanosine monophosphate, thereby closing cyclic nucleotide-gated channels[9,10] to produce well-characterized photoresponses.[2,11,12]

Retinitis pigmentosa (RP), a disease of progressive rod photoreceptor degeneration,[13] is caused by mutations in many genes. However, the rhodopsin mutation *P23H* is the most common cause of autosomal-dominant RP in North America.[14,15] In *Xenopus laevis* tadpoles expressing the bovine form of P23H rhodopsin (hereafter named bP23H), photoreceptors degenerate rapidly when exposed to cyclic light.[16–18] However, when reared in darkness, degeneration is prevented. Therefore, these animals have been used as a model for RP,[16,17,19,20] particularly the light-exacerbated retinal degeneration (RD) that likely occurs in cases of sector RP.[21–23] The exact mechanisms of toxicity remain unclear.

The *P23H* mutation promotes structural instability.[24] Previous studies suggest a mechanism involving destabilization of bP23H opsin by light, decreasing its exit from the ER.[25,26] In dark-reared *X. laevis*, expression levels of bP23H rhodopsin are low relative to the endogenous (wild type [WT]) rhodopsin, likely due to ER quality control. However, a significant quantity reaches the OS, resulting in expression levels of 7.5% relative to endogenous rhodopsin[16,26] (re-assessed for this study, see Supplemental Fig. S1). In dark-reared animals subsequently exposed to light, inner segment (IS) and OS membrane abnormalities rapidly develop.[18] Similarly, low basal expression, aggregation, and proteolytic degradation of P23H rod opsin expressed in the *Caenorhabditis elegans* neurons can be partially reversed by providing 9-cis retinal.[27]

P23H mutant mice have been examined using electroretinography (ERG), and showed abnormal a-waves.[28] At P40 they have abnormal ERGs and reduced rod nuclei numbers.[29] In the present manuscript, for the first time to our knowledge, we were able to probe phototransduction in intact retina and isolated rods from transgenic *X. laevis* expressing bP23H rhodopsin that were bred and housed in continuous darkness. We find that under these circumstances, unexpectedly bP23H-expressing rods do not degenerate and have almost normal photoresponses. In this way, we determined two early steps of the onset of RP and we quantified the number of photoisomerizations initiating these steps. The first step is caused by an exposure to light causing just a few photoisomerizations per disc and impairs phototransduction, although rods retain their integrity and morphology; the second step is initiated by a light exposure of 12 minutes causing rods to shed OS, lose their morphology, and degenerate. Therefore, RP in mutant rods is initiated by a very limited number of photoisomerizations.

Materials and Methods

Breeding and Rearing of Transgenic *X. Laevis*

X. laevis tadpoles carrying the *bP23H* transgene and expressing bP23H rhodopsin were generated by mating heterozygous or homozygous transgenic males with WT females.[16,17,19] WT tadpoles were derived from separate matings, or were siblings of transgenic tadpoles. Tadpoles were transferred to an 18°C to 21°C incubator that maintained 24-hr/d constant darkness. Expression levels were determined by dot blot assay as previously described[30] by determining the ratio of mAb 1D4 labelling (anti-mammalian rhodopsin, MAB5356; Millipore Sigma, Burlington, MA, USA) to B630N labeling (recognizes both mammalian and frog rhodopsin, gift of W. Clay Smith, University of Florida, Gainesville, FL, USA) relative to a standard containing both antibody epitopes and to nontransgenic retinas (Supplemental Fig. S1). All experiments adhered to the ARVO statement for the Use of Animals in Ophthalmic and Vision Research.

Isolation of Photoreceptors

Tadpoles and froglets were killed as previously described.[30] The developmental stage of each animal was determined (in the public domain, http://www.xenbase.org/anatomy/alldev.do). Eyes were enucleated and hemisected under infrared 820-nm illumination. Dissociated rods were obtained as reported.[31,32] Isolated intact rods obtained by mechanical dissociation were immersed in Ringer solution containing (in mM) 110 NaCl, 2.5 KCl, 1 $CaCl_2$, 1.6 $MgCl_2$, and 3 HEPES-NaOH, 0.01 EDTA, and 10 glucose (pH 7.7–7.8 buffered with NaOH). All chemicals were purchased from Sigma-Aldrich (St. Louis, MO, USA). All experiments were performed at 22°C to 24°C. Images were acquired using HCImage software 4.3.1.33 (Hamamatsu Corporation, Bridgewater, NJ, USA).

Single-Cell Photoresponse Recordings

After mechanical isolation, the IS of an isolated intact rod was drawn[33] into a silane-coated[34] borosilicate electrode (Blaubrand, intramark micropipette; BRAND GMBH + CO KG, Wertheim, Germany) (internal diameter of 4–6 μm) filled with Ringer's solution. Rods were viewed under 900-nm light using two cameras (Hamamatsu ORCA-Flash 4.0; Hamamatsu Corporation, Bridgewater, NJ, USA; and Jenoptic ProgRes MF; JENOPTIK I Optical Systems, Goeschwitzer, Jena, Germany) at two magnifications and stimulated with 491-nm diffuse light (Rapp OptoElectronic, Hamburg, Germany) from the ×10 objective of an inverted microscope (Olympus IX71; Olympus Corporation, Tokyo, Japan). To stimulate the entire OS, we used a stable continuous 491-nm laser module (for details see Mazzolini et al.[31]). Photoresponses were recorded as previously described[31] using an Axopatch 200A (Molecular Devices, LLC., San Jose, CA, USA) in voltage clamp-mode. The current was low-pass filtered at 20 Hz and digitized at 100 Hz. All recordings were processed, analyzed, and baselines corrected with Clampfit 10.3 (Molecular Devices). Data are expressed as mean ± standard error of the mean; single points represent single experiments.

Single-Photon Response Analysis

Single-photon responses were evoked by a series of 20 to 99 dim flashes delivered every 5 seconds, with duration of 10 ms. The data were fitted with the equations from reference from Baylor et al.[2] Threshold light intensities were tested on three *bP23H* and four WT rods at stages 55 to 59, one *bP23H* and two WT rods derived from froglets and on three WT rods derived from adults.

ERG Recordings

Dark-reared tadpoles (age 10 weeks, stage 56; offspring of a heterozygous transgenic and WT animal) or siblings exposed to cyclic light for 1 week, were anesthetized in 0.01% Tricaine in 0.1X MMR. ERG recordings to a series of 448-nm blue light flashes of increasing intensity from a light-emitting diode source were obtained as described by Vent-Schmidt et al.[35] The recording equipment incorporated a 1-Hz low-frequency cut-off filter and a 300-Hz high-frequency cut-off filter. Following ERG analysis tadpoles were genotyped to distinguish *bP23H* and WT animals as previously described.[35]

Confocal Microscopy

Eyes were fixed overnight at 4°C in 4% paraformaldehyde in 0.1 M phosphate buffer pH 7.4, and processed, cryosectioned, and labeled for confocal microscopy using Alexa488-conjugated wheat germ agglutinin (Invitrogen, Waltham, MA, USA) and Hoechst 33342 (Sigma, St. Louis, MO, USA) as previously described.[30] For transducin labeling, samples were fixed in 3.7% formaldehyde in 73% methanol. Polyclonal anti-alpha-transducin (gift of W. Clay Smith) and monoclonal anti-rhodopsin mAb 1D4 were used at 1:1000 dilution and detected with Cy3-conjugated anti-rabbit and anti-mouse secondary antibodies, respectively (Jackson Research, West Grove, PA, USA), as previously described.[30] Images were obtained using a Zeiss 510 meta confocal microscope equipped with a ×40 N.A. 1.2 water-immersion objective (Carl Zeiss, Oberkochen, Baden-Württemberg, Germany). Phagosomes were identified by morphology by a blinded lab member. Phagosome area was quantified using ImageJ software (http://imagej.nih.gov/ij/; provided in the public domain by the National Institutes of Health, Bethesda, MD, USA).[36]

Estimation of the Number of Photoactivated bP23H Rhodopsins (Rh*) on a Disc

Assuming 25,000 Rh/μm^2 one *bP23H* disc has an area of 12.6 μm^2 (based on a diameter of 4 μm) giving 25,000 Rh/$\mu m^2 \times 12.6\ \mu m^2 = 3.15 \times 10^5$ Rh/disc.[11] There are 2100 discs/rod in toad[11] with a length of 60 μm. Our observed *bP23H* OS length is 33 μm, therefore 1155 discs. The total Rh/rod = $1155 \times 3.15 \times 10^5 = 3.6 \times 10^8$. In dark-reared animals, bP23H Rh is 7.5% of the total[19] giving an estimated number of bP23H Rh per rod of 2.7×10^7 (bP23H Rh 2.36×10^4 per disc).

Considering our lower limit of photoisomerization to see an effect on phototransduction of 60,000 Rh* in 30 to 60 minutes, we have $60{,}000/3.6 \times 10^8 = 0.00017$ Rh*/Rh (2 Rh* every 10,000 Rh); considering our upper limit of 500,000 Rh* in approximately 6 minutes we have the following: $500{,}000/3.6 \times 10^8 = 0.0014$ Rh*/Rh (1.4 Rh* every 1000 Rh). Therefore, we obtain in the former case 4 bP23H Rh* per disc (0.00017 Rh*/Rh $\times 2.3 \times 10^4$ bP23H Rh/disc), in the latter 32 bP23H Rh* per disc (0.0014 Rh*/Rh $\times 2.3 \times 10^4$ bP23H Rh*/disc).

Results

X. Laevis Carrying the *bP23H* Transgene Have a Rapid Light-Induced RD

As previously reported,[16–18,26] *X. laevis* tadpoles expressing bP23H rhodopsin show no detectable RD when reared in complete darkness for up to 10 weeks. However, when exposed to 1700-lux cyclic light for 1 week, RD occurs rapidly (Fig. 1A). Our transgenic line expresses bP23H rhodopsin in rods uniformly throughout the retina at 7.5% of the level of

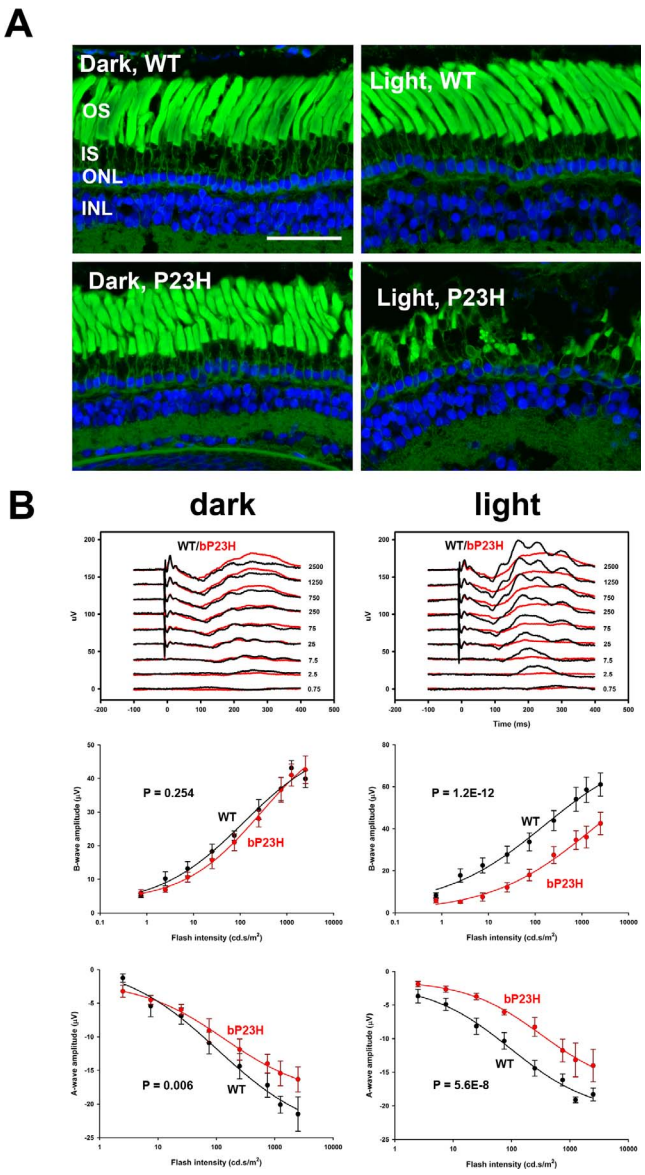

Figure 1. Histology and electroretinography of WT and *bP23H* tadpoles reared in darkness or exposed to 1 week of cyclic light. (**A**) Confocal micrographs stained with wheat germ agglutinin (*green*) and Hoechst 33342 nuclear stain (*blue*). There is no evidence of retinal degeneration in dark-reared *bP23H* animals relative to WT, while *bP23H* animals transferred to cyclic light for 1 week have few remaining rods. (**B**) Electroretinography of WT and *bP23H* animals housed under the same conditions as in (**A**) showing averaged traces (*top*) and A- and B-wave analysis (below). *bP23H* results are shown in red, and WT results are shown in *black*. *Error bars* are ± SEM. For dark-reared conditions (*left*) *bP23H* $n = 8$ and WT $n = 8$. For light-exposed animals (*right*) *bP23H* $n = 7$ and WT $n = 5$. *P* values shown on charts represent the statistical significance of the effect of genotype in a two-way ANOVA analysis (intensity versus genotype). The effect of intensity was highly significant in all cases ($P < 10^{E-12}$). The sharp peaks seen in the first 50 ms following the flash are recording artefacts.

endogenous rhodopsin[16] (Supplemental Figs. S1 and S2). Therefore, these animals present a unique opportunity to examine the electrophysiology of nondegenerating rods expressing relatively large quantities of a disease-causing rhodopsin mutant, as well as the initial physiological alterations of rods undergoing RD induced by light.

Dark-Reared *X. Laevis* Carrying the *bP23H* Transgene Have Relatively Normal ERG Responses

We compared ERG recordings from *bP23H* and WT tadpoles (Fig. 1B). For animals reared 10 weeks in darkness, *bP23H* recordings (red traces) were similar to WT (black traces). Although B-wave amplitude appeared slightly lower in *bP23H* tadpoles, we found no statistically significant effect of genotype. A-wave amplitudes were similar between the two groups, but smaller in *bP23H* animals at high flash intensities (2-way ANOVA, $P = 0.006$ for effect of genotype). In contrast, after 1 week in cyclic light, A- and B-wave amplitudes were markedly different between genotypes (effect of genotype for B-wave, $P = 1.2^{E-12}$, A-wave, $P = 5.6^{E-8}$) consistent with significant RD.

Conversion From Arbitrary Units to Photoisomerizations Through Single-Photon Analysis

For single-cell photoresponse recordings, we calibrated our laser illumination from arbitrary units (AU) to induced photoisomerizations (Rh*) per rod by performing single-photon analysis[2] of mutant (Figs. 2A–C) and WT rods (Figs. 2D–F) obtained from tadpoles and froglets kept in constant darkness and WT rods obtained from adults kept in cyclic light (Figs. 2G–I) and estimated the number of rhodopsin molecules activated by a given flash intensity.[2] We established that our dimmest flash of 50 AU, with a duration of 10 ms, generated 1.5 to 2.5 photoisomerizations with a mean response amplitude of approximately 0.5 pA. We use this conversion throughout the manuscript (see Methods). Our *X. laevis* single-photon response is slightly lower than previously reported and both estimates are lower than reported for adult *Bufo* rods.[2,37,38]

Transgenic *X. Laevis* Reared in Darkness Have Almost Normal Phototransduction Machinery

We carried out single-cell suction-electrode recordings from isolated rods from WT (Fig. 3A) and *bP23H* (Fig. 3B) tadpoles reared in darkness.

Isolated WT and *bP23H* rods responded to flashes of increasing intensity with a decrease of the circulating current where the maximal amplitude reflects the size of the dark current (Figs. 3C, 3D) as previously described for adult *X. laevis* rods.[31] The maximal amplitude (I_{dark}) varied between developmental stages (Figs. 3C, 3D and the Table) as previously observed in WT *X. laevis* rods[37,38] and between WT and *bP23H* rods. For a given developmental stage, *bP23H* rods produced 35% lower maximal photoresponses than WT rods. When normalized to their maximal amplitude (Fig. 2E), the rising phases of WT and *bP23H* photoresponses (black versus red traces) were superimposable (red traces) and had a similar time course and time to peak (Fig. 3F and the Table).

An analysis of WT and mutant rod geometry showed that WT OS were 11 μm longer and 0.5 μm wider than *bP23H* OS (Table). Therefore, the ratio of the OS surface area between *bP23H* and WT rods is approximately 0.6, in good agreement with the maximal photoresponse ratio. We also compared the relation between the normalized photoresponse amplitude (R/R_{max}) and light intensity (Fig. 3H), fitted by a Michaelis-Menten equation (see the Table). The $I_{1/2}$ value for *bP23H* was half that of WT, indicating reduced sensitivity. The relation between the maximal amplitude R_{max} and OS length was approximately linear for both *bP23H* and WT rods (Fig. 3H).

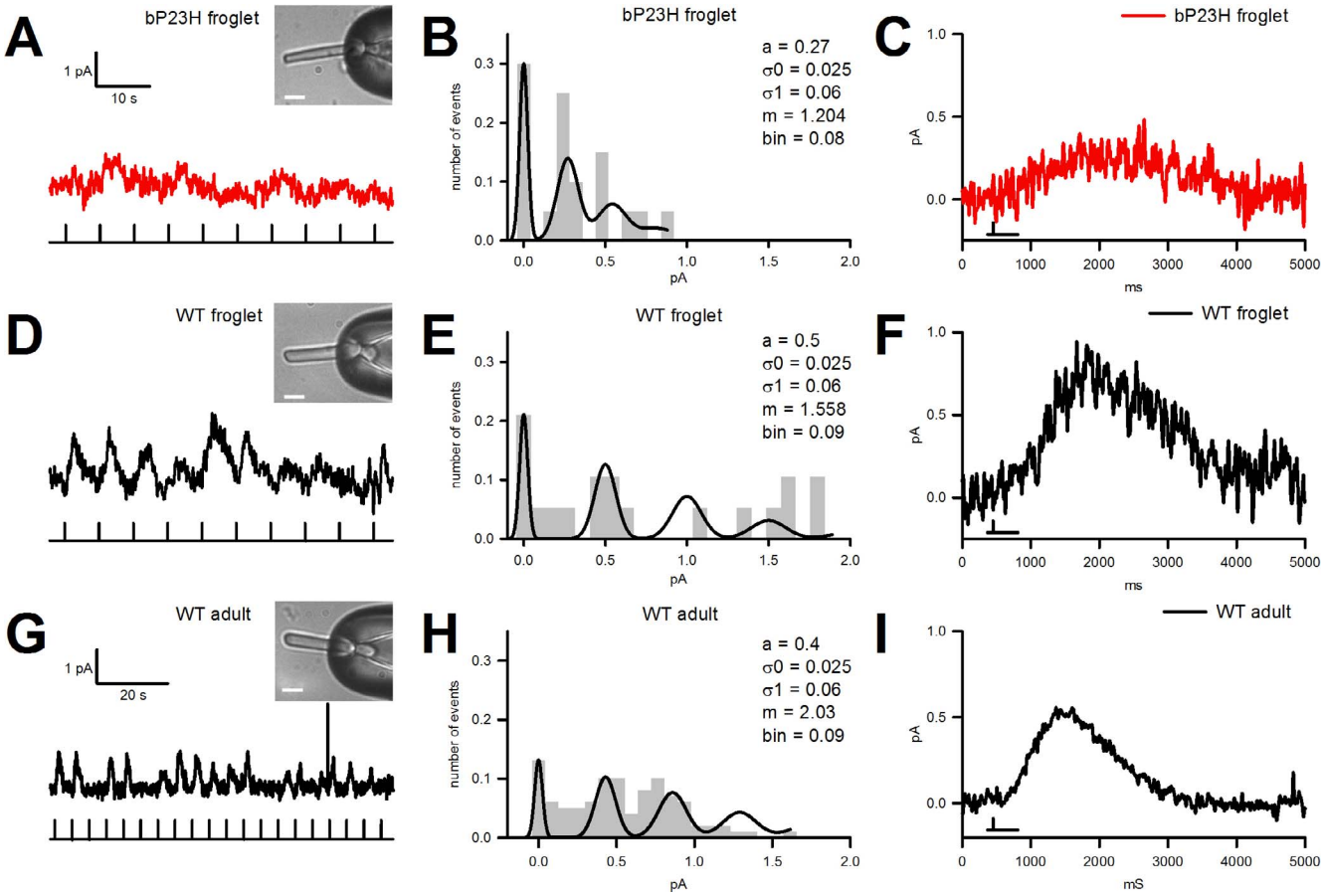

Figure 2. Single-photon analysis of a *bP23H* and WT rod, obtained from tadpoles kept in constant darkness, and a WT rod obtained from an adult kept in cyclic light. (**A**, **D**) Photoresponses elicited by diffuse dim flashes of light, evoking 1.5 to 2.5 Rh* for a mutant (*red*), a WT (*black*) rod, respectively. *Insets* represent the rods, with the IS inside the electrode (*scale bar*, 10 μm). **(G)** The same as (**A**) and (**D**) but for a WT adult kept in cyclic light. (**B**, **E**) Histograms of the amplitudes of evoked photoresponses ($n = 20$). (**H**) The same as (**B**) and (**E**) but for a WT adult kept in cyclic light ($n = 99$). The histograms were fitted with the equation described in Materials and Methods. Values providing the best fit are reported in the panel; 'a' is the mean response to single photon, 'σ0' is the noise SD, 'σ1' is the SD of the mean, and 'm' is the mean number of events per trial. (**C**, **F**) Averages of the evoked photoresponse to diffuse dim flashes of light in (**A**) and (**D**), respectively. (**I**) The same as (**C**) and (**F**) but for a WT adult kept in cyclic light.

We also recorded photoresponses from tadpoles maintained in a single 12-hour light/12-hour dark cycle. WT rods displayed normal morphology and responses (Figs. 3I, 3K), whereas the responses and morphology of the (very few) remaining *bP23H* rods were altered (Figs. 3J, 3L).

We investigated the rising (Fig. 4A) and falling phases (Fig. 4B) of photoresponses from WT and *bP23H* rods (black versus red traces) following normalization to the maximal photoresponse. The photocurrent rapidly decreased (rising phase) after the application of bright flashes, with matching kinetics for WT and *bP23H* (Fig. 4A). In addition, the time course of the falling phase for WT and *bP23H* was very similar (Fig. 4B). We also compared the initial phase of light adaptation during exposure to either repetitive flashes or longer pulses.[39] The time course of photoresponses to 10 consecutive flashes separated by 1 and 2 seconds was remarkably alike (Figs. 4C, 4D). Complementary results were observed when 20-second pulses were considered (Fig. 4E). Additionally, we observed a delayed photoresponse decline associated with the onset of light adaptation in both WT and *bP23H* rods, indicating the initial steps of light adaptation were congruent (Fig. 4G).

The Phototransduction Machinery in *bP23H* Rods is Impaired Following Saturating Light Exposures

We know that RD occurs if *bP23H* transgenic animals are reared in light, but how many photons are necessary to trigger degeneration? Is the phototransduction machinery impaired before rod collapse? We exposed WT and *bP23H* rods to light and estimated the number of Rh* while recording photoresponses. In the majority of WT recordings, photoresponse amplitudes, and time courses were stable over 30 to 60 minutes. In some cases, it was possible to record photoresponses with the same maximal amplitude for 1 hour or longer. Figure 5A shows an initial WT photoresponse to a bright flash (black trace) and responses after 47, 74, and 128 minutes (gray and pale gray traces). The morphology of the rod did not change significantly during recording (see inset of Fig. 5A and Figs. 6A–D). Figure 5B shows a similar experiment with a *bP23H* rod: in contrast to WT, the photoresponse was prolonged after approximately 60 minutes of continuous recording (compare red and dark red traces). With time, the photoresponse amplitude declined and the time course was further prolonged (red and pale red traces in Fig. 5B). Again, the morphology did not change appreciably (see Figs. 5B, inset,

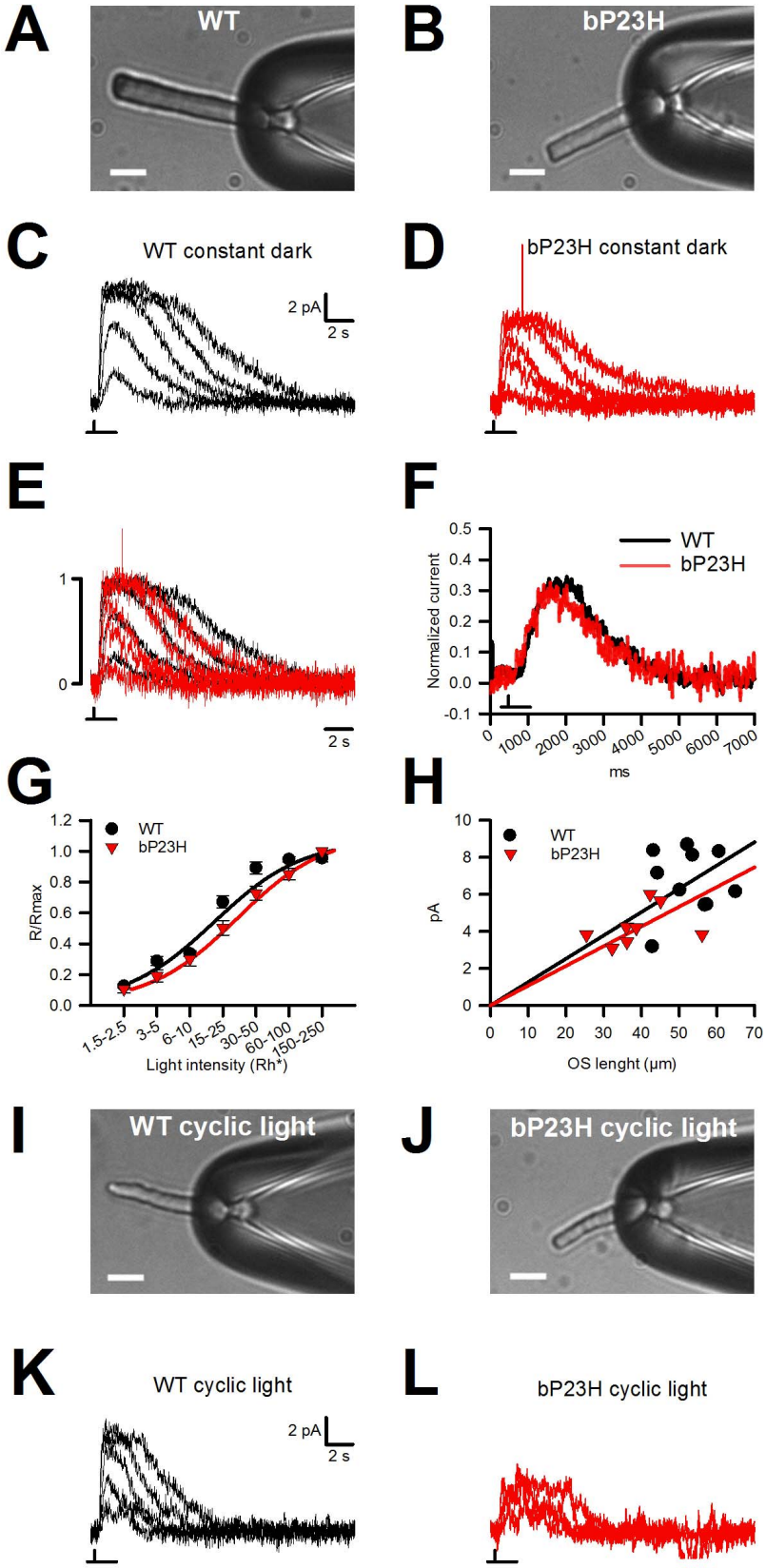

Figure 3. Comparison of photoresponses of WT and *bP23H* rods. (**A**, **B**) Isolated rods from a WT and a *bP23H X. laevis* tadpole, respectively. (**C**) A family of photoresponses to diffuse light of increasing intensity for the WT rod in (**A**). The maximal amplitude of current is 8.7 pA for a flash inducing 150 to 250 Rh*. The flashes were applied at the time indicated by the *black bar* and had a duration of 10 ms. The light intensity produced by the laser was equivalent to 6 to 10, 15 to 25, 30 to 50, 60 to 100, and 150 to 250 Rh*, respectively. The photoresponses of WTs' rod had a maximal amplitude of 6.5 ± 0.5 pA ($n = 2$) at stage 49 to 54, 7.0 ± 0.7 pA ($n = 7$) at stage 55 to 59 and 13.4 ± 1.1 pA ($n = 6$) starting from the stage

66 (froglets-adult stage) of development. (**D**) Example of a family of photoresponses as in (**C**) but for the *bP23H* rod in (**B**). The maximal amplitude of current is 6.0 pA for a flash inducing 150 to 250 Rh*. The photoresponses of *bP23H* rods increased with development and was approximately 3.6 ± 0.2 pA ($n = 3$) at stage 49 to 54, 4.9 ± 0.5 pA ($n = 4$) at stage 55 to 59 and increased to 7.2 ± 1.2 pA ($n = 7$) pA starting from the stage 66 (froglets-adult stage) of development. (**E**) Superimposition of normalized photocurrent in (**C**) (*black*) and in (**D**) (*red*). (**F**) Superimposition of normalized dim flashes, eliciting 6 to 10 Rh*, from 10 WT and 8 *bP23H* rods (developmental stage 49–60). (**G**) Comparison of the relation between the normalized amplitude of photoresponses (R/R_{max}) and light intensity (I) for WT (black circle; $n = 3$–10) and *bP23H* (*red triangles*; $n = 3$–8). The data were fitted with the equation $R/R_{max} = I/(I + I_{1/2})$ where $I_{1/2}$ is equivalent to 10 to 16 Rh* ±1 for WT (*black line*) and to 16 to 27 Rh* ±2 for mutants (*red line*). (**H**) Relation between OS length and saturating current for WT (*black circles*; n = 10) and *bP23H* (*red triangles*; $n = 8$). The data were fitted with a linear regression $R_{max} = c^*l$, with a value of 0.13 and 0.11 of c for WT and *bP23H* rods, respectively. (**I**, **J**) Isolated rods from a WT and a *bP23H X. laevis* tadpoles that were exposed to a single 12-hour light/12-hur dark cycle. (**K**) Family of photoresponses from the rod in (**I**) elicited by 6 to 10, 15 to 25, 30 to 50, 60 to 100, and 150 to 250 Rh*, respectively. The maximal amplitude of current is 6.9 pA for a flash inducing 150 to 250 Rh*. (**L**) Family of photoresponses of the rod in (**J**) elicited by 15 to 25, 30 to 50, 60 to 100, and 150 to 250 Rh*, respectively. The maximal amplitude of current is 3.6 pA for a flash inducing 150 to 250 Rh*. In (**A**, **B**, **I**, **J**) the *scale bars* represent 10 μm.

and 6E–H). We compared variation in amplitude (Fig. 5C) and duration (Fig. 5D) of the maximal response with time for WT (black dots, $n = 3$) and *bP23H* rods (red triangles, $n = 3$): *bP23H* photoresponses declined and were prolonged after approximately 60 minutes. We also averaged photoresponses ($n = 7$) from different *bP23H* rods at the beginning of recording (dark red) and after tens of minutes (red trace in Fig. 5E). This averaging confirmed decreased amplitude and prolongation of the photoresponse.

We observed prolongation of *bP23H* rod photoresponses after tens of minutes and the occurrence of between 6×10^4 and 1×10^5 Rh* (Figs. 5B, 5D, 5E). To distinguish whether this was due to elapsed time or the number of Rh*, we delivered our standard bright flash and after 2 to 3 minutes, exposed the rod to a 1-second step of light with the same intensity, evoking 5×10^5 Rh* of Rh* (Figs. 5F, 5H). In WT rods, when the standard flash was re-delivered, the photoresponse time course was accelerated (compare black and gray trace in Fig. 5G). In contrast, in *bP23H* rods, the photoresponse was prolonged (compare the dark red and red traces in Fig. 5I) and its amplitude often declined. The time course and duration of subsequent photoresponses were further prolonged (pale red trace in Figs. 5I and 6E–H). Thus, when *bP23H* rods are exposed to light of different durations but evoking a total number of Rh* varying from 6×10^4 to 5×10^5 Rh*, the phototransduction machinery is altered. In dark-reared rods the fraction of bP23H rhodopsin is approximately 7.5%[16,26] (Supplemental Fig. S1), therefore the total amount of bP23H rhodopsin per disc is 2.3×10^4 (see Methods). We estimate that the total number of discs in a *bP23H* rod is approximately 1100, based on the total number of discs in a toad rod (2100 discs/rod in toad, length 60 μm; *bP23H* OS length 33 μm;

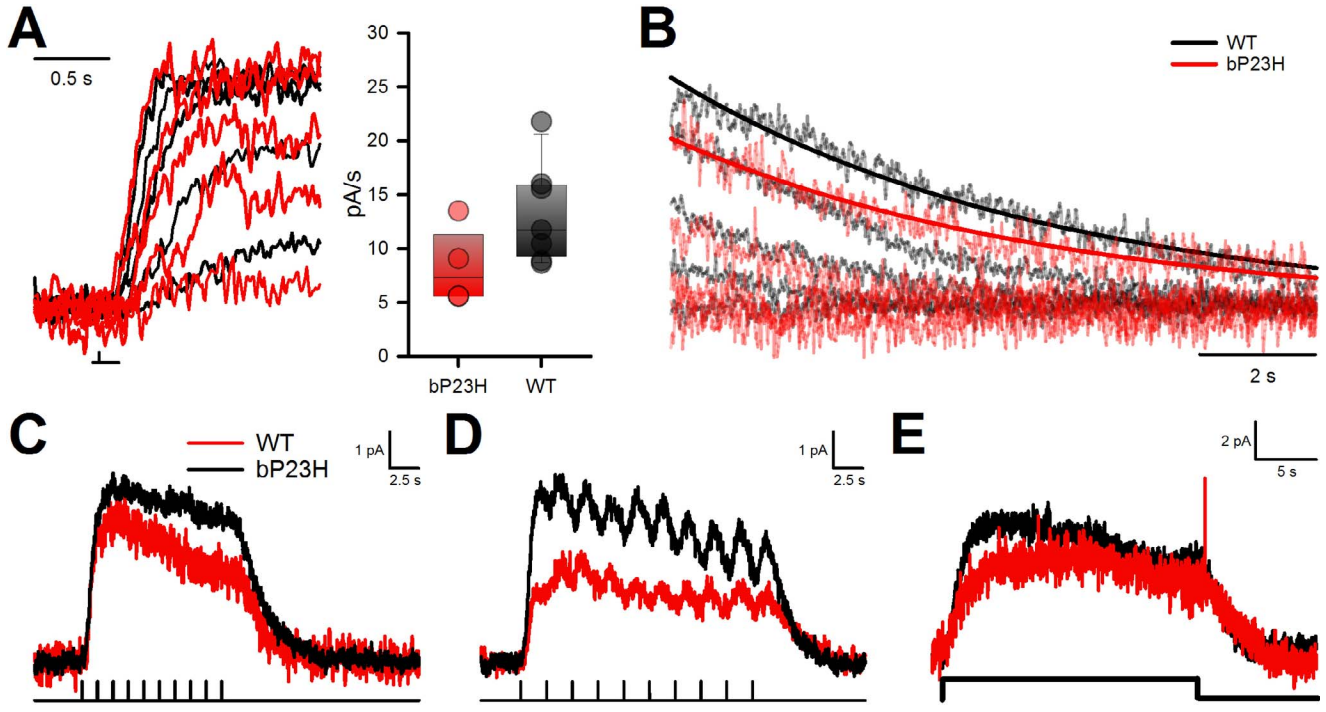

Figure 4. Comparison of rising/falling phases of *bP23H* and WT photoresponses. Analysis of light-adaptation response to repetitive flashes and step of light, WT, and *bP23H* rods. (**A**) Expanded scale for families of selected photoresponses to normalized diffuse light (Fig. 1E) of increasing intensity of a WT (*black traces*) and *bP23H* rods (*red traces*) showing the rising phase. The histograms represent the collective data for the activation rate of the saturating responses of *bP23H* ($n = 4$) and WT ($n = 7$) tadpoles at stages 55 to 59. (**B**) The same as in (**A**) but for the falling phase. *Black* and *red continuous lines* are exponential decay fittings with the equation $y = ae^{-bx}$. Coefficient a was 3.1 for the *bP23H* fitting and 2.3 for the WT. (**C**) Averaged photoresponses evoked from 10 identical nonsaturating light flashes with a duration of 10 ms, equivalent to 150 to 250 Rh* applied with a time interval (Δt) of 1 s for the WT (*black traces* $n = 7$) and for the *bP23H* (*red traces* $n = 3$). (**D**) As in (**C**) but for photoresponses evoked with a Δt of 2 s (black traces $n = 6$ and red traces $n = 7$). (**E**) Example of photoresponse to a step of light with a duration of 20 s in nonsaturating light conditions for WT (*black traces*) and *bP23H* (*red traces*) equivalent to 15 to 25 Rh*/sec and 30 to 50 Rh*/sec, respectively.

TABLE. Various Parameters of WT and *bP23H* Rods

Genotype Condition	Rod Length, μm	OS, μm	Diameter, μm	I_{dark}, pA	$I_{1/2}$, Rh*	$S_{f(\infty)}$, 1/Rh*	T_{peak}, ms	T_{integr}, ms
WT	51.5 ± 1.3 (38)	44.8 ± 1.2 (38)	5.1 ± 0.1 (38)	7.4 ± 0.5 (7)	10 to 16 (7)	$3.7 \times 10^{-2} \pm 0.3 \times 10^{-3}$ to $6.2 \times 10^{-2} \pm 0.5 \times 10^{-3}$ (7)	1135 ± 108 (7)	3429 ± 222 (7)
bP23H	39.7 ± 0.7* (70)	33.6 ± 0.6* (70)	4.7 ± 0.1† (70)	5.3 ± 0.6* (4)	16 to 27 ± 2‡ (4)	$2.1 \times 10^{-2} \pm 0.3 \times 10^{-3}$ to $3.5 \times 10^{-2} \pm 0.5 \times 10^{-3}$‡ (4)	1009 ± 150 (NS) (4)	2623 ± 323† (4)
WT cyclic light	40.2 ± 1.2 (3)	34 ± 1.2 (3)	4.2 ± 0.4 (3)	6.2 ± 0.5 (3)	//	//	908 ± 117 (3)	3590 ± 137 (3)
bP23H cyclic light	31.4 ± 4.7 (2)	25.3 ± 5.1 (2)	4.2 ± 0.4 (2)	3 ± 0.5 (2)	//	//	797 ± 86 (2)	1580 ± 78 (2)

I_{dark}, light-saturated responses dark current; $I_{1/2}$, light intensity necessary to obtain a response that is half of the saturating response; $S_{f(\infty)}$, is the fractional sensitivity of the normalized dim flash, calculated as the amplitude of the dim flash response divided by its strength and then normalized for the amplitude of the saturating response; T_{peak}, time to peak of a dim flash response with an amplitude of approximately 0.2 of the I_{dark}; T_{integr}, integration time and it is estimated as the integral of dim-flash responses (with amplitudes of ~0.2 I_{dark}) normalized to its peak amplitude; NS, not significant.

Values shown are mean ± SEM.

* <0.001, compared with WT values.

† <0.05, compared with WT values.

‡ <0.01, compared with WT values.

number of discs = 33 × 2100/60 = 1155). Therefore, the occurrence of just 4 to 32 bP23H photoisomerizations/disc is sufficient to impair phototransduction machinery.

Short-Light Exposures Trigger OS Shedding in *bP23H* Rods

Within hours of exposing *bP23H* animals to light, RD, including OS morphologic changes, is initiated.[18] To determine the minimum exposure required, we exposed *bP23H* animals to varying periods of bright light and returned them to darkness before euthanizing them, for a total period (light + dark) of 4 hours. We found that exposures of 12 minutes or longer induced massive shedding of *bP23H* rods into the RPE that was apparent by 4 hours (Fig. 7). Both the number and area of RPE phagosomes increased dramatically after light exposure (Figs. 7A, 7C) indicating disruption of OS. To verify that we employed a rod-saturating intensity, we examined alpha-transducin migration in light-exposed WT animals (Fig. 7B). At rod-saturating intensities, alpha-transducin distribution alters from an exclusively OS localization to a combined OS/IS localization due to saturation of PDE binding.[40,41] As alpha-transducin partially migrated to ISs, our standard illumination was rod saturating.

We estimated the total number of Rh* required to induce disc shedding in *bP23H* tadpoles in two different ways and arrived at similar conclusions. Transducin migration indicates that 1700 lux is sufficient to saturate photoresponses, which in our single-rod experiments occurred with flashes of light producing from 100 to 250 Rh* per rod. If the same photon flux is prolonged from 10 ms to 12 minutes the total number of induced Rh* per rod is equivalent to 7.2×10^6 to 1.8×10^7. Based on analysis of ERG a-wave data from *bP23H* tadpoles (Fig. 1B), we found that half-maximal retinal stimulation occurred at a value of 126 lux, equating to the value of 16 to 27 Rh* per *bP23H* rod shown in the Table. Thus, 12 minutes of constant 1700-lux light would be predicted to generate 1.55 to 2.6×10^7 Rh*. Based on these methodologies, we estimate that the number of Rh* leading to disk shedding in *bP23H* rods is in the range of 7.2×10^6 to 2.6×10^7 Rh* (from 460–1610 bP23H Rh* per disc).

DISCUSSION

The present manuscript reveals three major and novel findings in rods bearing the *P23H* mutation, the leading cause of RP. First, if *X. laevis* tadpoles carrying the rhodopsin *P23H* mutation are reared in darkness, mutant rods have functional and almost normal phototransduction machinery. Second, when exposed to a bright light lasting 1 second (Fig. 4), their photoresponses are irreversibly prolonged. Third, when light exposure is maintained for 12 minutes (Fig. 5), significant OS shedding occurs and RD is initiated. Therefore, the first step leading to RD is the prolongation of photoresponses associated with the photoisomerization of 6×10^4 to 5×10^5 Rh*, equivalent to 4 to 32 P23H rhodopsins per disc. However, initiation of dramatic morphologic changes identifiable by light microscopy, such as OS shedding, requires 1 to 2 orders of magnitude greater Rh*. How can we account for this extreme sensitivity? While previous phototransduction models were based on freely diffusing rhodopsin, recent studies indicate that rhodopsins—and presumably bP23H rhodopsin—are organized in discs along parallel tracks of dimers.[42–45] Signal amplification requires multiple diffusion encounters, likely involving rhodopsins anchored in tracks of dimers while other phototransduction components diffuse more freely.[42,46] The photoresponse prolongation observed in *bP23H* rods is

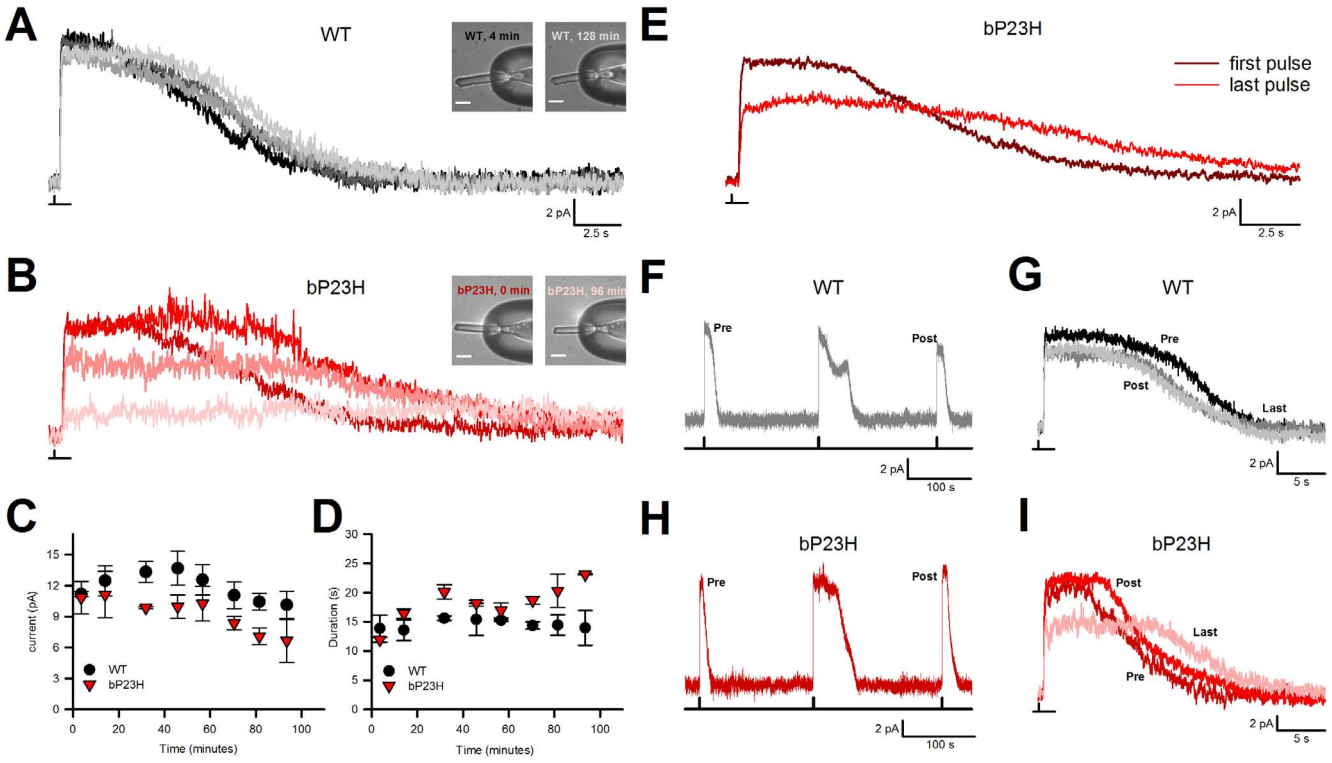

Figure 5. Comparison of the photoresponses of WT and *bP23H* rods to prolonged or acute exposure of saturating light (developmental stage 60–66). (**A**) Examples of photoresponses evoked by identical saturating flashes (100k AU, equivalent to 3×10^3 to 5×10^3 Rh*) with a duration of 10 ms applied at the beginning of the experiments (*black traces*) and at specific time interval (*gray traces*) for a WT rod. In the *inset*, the correspondent isolated rod from WT *X. laevis* froglet at the beginning (0 min) and at the end (128 min) of the experiment. (**B**) Examples of photoresponses evoked by identical saturating flashes as in (**A**), applied at the beginning of the experiments (*dark red traces*) and at specific time interval (*red traces*) for a *bP23H* rod. In the *inset*, the correspondent isolated rod from *bP23H* rod *X. laevis* froglet at the beginning (0 min) and at the end (96 min) of the experiment. (**C**) Plot representing the variation of maximal current amplitude (in pA) in relation to different time along the experiment (WT and *bP23H* rods, $n = 3$). (**D**) Plot representing the elongation of saturation time (in pA) in relation to different time along the experiment (WT and *bP23H* rods, $n = 3$). (**E**) Averaged photoresponses for the *bP23H* rods at the beginning (*dark red trace*, $n = 7$) and at the end (*light red trace*, $n = 7$) of the experiment. (**F**) Example of photoresponses of WT rods evoked by identical saturating flashes (equivalent to 3×10^3 to 5×10^3 Rh*) with a duration of 10 ms applied before (pre) and after (post) a step (in the middle) with a duration of 1 second (equivalent to 3×10^5 to 5×10^5 Rh*). (**G**) Superimposition of photoresponses of WT rods evoked by identical saturating flashes (equivalent to 3×10^3 to 5×10^3 Rh*) with a duration flash of 10 ms applied at the beginning (pre), in the middle (post) and at the end of the experiment (last). (**H**) The same as in (**F**) but for a *bP23H* rod. (**I**) The same as in (**G**) but for *bP23H* rod. In all *insets scale bar*, 10 μm.

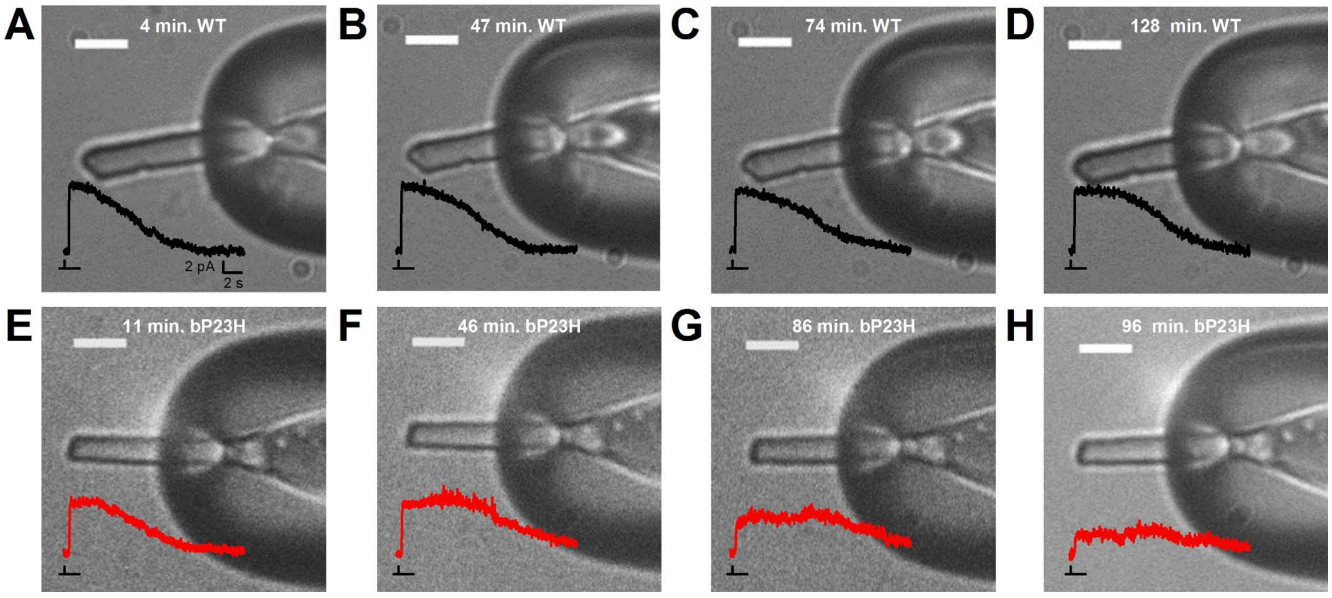

Figure 6. *bP23H* rods display the same morphology during multiple saturating light stimulations. (**A–D**) Monitoring of a WT rod morphology through time (same rod as in Fig. 5A). The traces represent examples of photoresponses to saturating flashes of light equivalent to 3×10^3 to 5×10^3 Rh*, shortly before/after the associated pictures. (**E–H**) Monitoring of a *bP23H* rod morphology through time (same rod as in Fig. 5B). The traces represent examples of photoresponses to saturating flashes of light equivalent to 3×10^3 to 5×10^3 Rh*, shortly before/after the associated pictures.

Investigative Ophthalmology & Visual Science

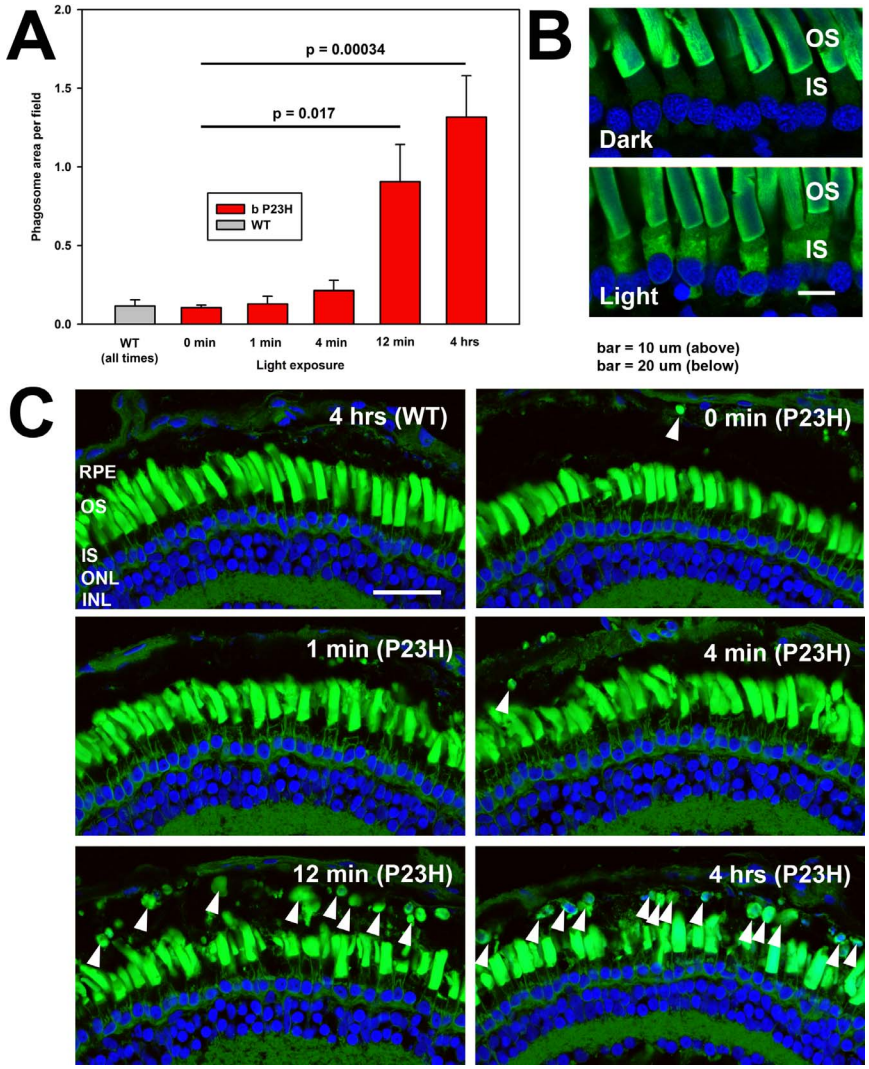

Figure 7. Titration of light exposures sufficient to induce retinal degeneration in *bP23H* tadpoles: *bP23H* and WT tadpoles were reared in complete darkness and exposed to bright light (1700 lux) for the indicated periods, and then returned to darkness, for a total time of 4 hours. (**A**) Plots representing quantitative data of phagosome structures expressed in terms of phagosome area. *P* values shown on the plots were obtained using Dunnet's test for multiple comparisons following ANOVA. (**B**) High-magnification panels showing that transducin localization changes on light exposure, indicating that 1700 lux is a rod-saturating light intensity. *Green*: antialpha-transducin; *blue*: Hoechst 33342 nuclear stain. (**C**) Confocal micrographs of cryosectioned retinas corresponding to plot (**A**). A 12-minute light exposure is sufficient to induce significant retinal degeneration including abundant shedding of photoreceptor OS into the RPE (*arrowheads*). In contrast, exposures of 4 minutes or less did not induce significant retinal degeneration, and WT retinas were unaffected. *Green*: Wheat germ agglutinin; *blue*: Hoechst 33342 nuclear stain. *Scale bar*, 10 μm (**B**) or 40 μm (**C**).

consistent with impaired rhodopsin shutoff. Transducin GTPase, arrestin, rhodopsin kinase, and RGS9 are involved in phototransduction shutoff and could have roles in this impairment.

The residue P23 is located on the intradiscal face of rhodopsin in the N-terminal domain of the protein.[45,47] The majority of the bP23H rhodopsin that evades quality control and reaches the OS is proteolytically processed to remove a portion of the N-terminal domain. This portion includes the N-terminal glycosylation sites, (most likely) the P23H residue itself,[16] and a hydrophobic cluster that is essential for the structural stability of the entire protein.[27] Therefore, OS bP23H rhodopsin is structurally destabilized, either by insertion of a missense amino acid, or removal of the N-terminus.

Structural destabilization of bP23H rhodopsin could result in aggregation or alterations of track structures that trap activated transducin, or prevent normal interactions of cascade shutoff proteins, effectively impairing not only transduction initiated by bP23H rhodopsin, but also transduction initiated by WT rhodopsins in the same or adjacent tracks. Another possibility is that an alternate bP23H rhodopsin structure is induced by interaction with WT meta-II rhodopsin. Thus, it is possible that upon light exposure, bP23H rhodopsin adopts an alternate conformation that alters not only the structure of the N-terminus, but also the domains that interact with signal transduction components. Under these conditions, a small impairment of the shutoff of bleached mutant *P23H* rhodopsins could lead to a noticeable prolongation of the photoresponse as experimentally observed (Fig. 4).

A rod-saturating exposure lasting 12 minutes induces OS shedding in mutant *bP23H* rods but not in WT rods (Fig. 5). Based on two different calculations, the number of Rh* leading to OS shedding in *bP23H* rods ranges from 7.2×10^6 to 2.7×10^7 per rod, or 460 to 1610 bleached bP23H rhodopsins per

disc, which could aggregate with other rhodopsins, possibly altering local membrane fluidity and slowing local phototransduction shut off. Indeed, the specific organization of rhodopsins in tracks of dimers[42] is likely to be compromised by the misfolding of very few, and possibly even 4 to 32, bleached *bP23H* rhodopsin, while the presence of some hundreds to thousands of misfolded P23H rhodopsins dramatically disrupts OS architecture and could lead to OS shedding.

Single-cell recordings from photoreceptors in animal models of RD are rare because of difficulty in acquiring the data.[28,48,49] In 2-week-old mutant *P23H* mice reared in a standard light cycle, it is difficult to identify rod OS even at the retinal margin because of severe RD. However, *X. laevis* models of RP are well suited to this purpose due to the larger size of their rods, and the availability of several RP models in which RD can be dramatically limited by dark rearing.[16,30,50–52]

Light-exacerbated RD has been reported in P23H rats and fruit flies, and is strongly suggested by the sector RP phenotype reported in human patients. Similar to P23H *X. laevis*, expression levels of P23H rhodopsin in knockin mice is low due to a biosynthetic defect,[28,53] and the accumulation of mutated rhodopsin in the ER has been associated with cell stress, activation of the unfolded protein response, the activation of the ubiquitination system and ER-associated degradation.[54,55] While it is generally thought that ER stress–based mechanisms are responsible for the resulting RD, exacerbating ER stress by light exposure should require timeframes that would allow biosynthesis of significant quantities of rhodopsin, rather than the rapid timeframes of seconds to minutes seen in our study. Interestingly, pharmacologic treatment of P23H mice with metformin, which promotes delivery of P23H rhodopsin to the OS, exacerbates RD.[56] Therefore, OS-based mechanisms may contribute to cell death in both *X. laevis* and other species, and may be favored under certain conditions. Moreover, results consistent with abnormal rod responses have been observed in RP patients carrying the *P23H* mutation or other mutations causing sector RP, including an altered and prolonged dark-adaptation phase after the light stimuli, suggesting an altered recovery phase of rod response.[23,57,58] Similar findings were reported regarding ERG measurements obtained from P23H (*VPP*) transgenic mice.[59] It will be interesting to determine whether the effects we observed are common to multiple mutations or unique to P23H rhodopsin.

Acknowledgments

The authors thank M. Lough for proofreading. We thank Matteo Caorsi (SISSA Mathematics Area) for the help with the calculations and Marco Gigante for the three-dimensional printed recording chamber (SISSA Mechatronic lab) and W. Clay Smith for gifts of antibody reagents. A special thanks to Monica Mazzolini for her useful advice, her comments on the manuscript, and for her help with the analysis of the data.

Supported by grants from the Foundation Fighting Blindness (OLM, Toronto, Canada), the Canadian Institutes of Health Research (OLM, PJT-156072; Ottawa, ON, Canada), and the Natural Sciences and Engineering Research Council of Canada (OLM, RGPIN-2015-04326; Ottawa, ON, Canada).

Disclosure: **U. Bocchero**, None; **B.M. Tam**, None; **C.N. Chiu**, None; **V. Torre**, None; **O.L. Moritz**, None

References

1. Yoshizawa T, Wald G. Pre-lumirhodopsin and the bleaching of visual pigments. *Nature*. 1963;197:1279–1286.
2. Baylor DA, Lamb TD, Yau KW. Responses of retinal rods to single photons. *J Physiol*. 1979;288:613–634.
3. Kwok-Keung Fung B, Stryer L. Photolyzed rhodopsin catalyzes the exchange of GTP for bound GDP in retinal rod outer segments. *Proc Natl Acad Sci U S A*. 1980;77:2500–2504.
4. Molday RS, Moritz OL. Photoreceptors at a glance. *J Cell Sci*. 2015;128:4039–4045.
5. Fotiadis D, Liang Y, Filipek S, Saperstein DA, Engel A, Palczewski K. The G protein-coupled receptor rhodopsin in the native membrane. *FEBS Lett*. 2004;564:281–288.
6. Baehr W, Devlin MJ, Applebury ML. Isolation and characterization of cGMP phosphodiesterase from bovine rod outer segments. *J Biol Chem*. 1979;254:11669–11677.
7. Dumke CL, Arshavsky VY, Calvert PD, Bownds MD, Pugh EN. Rod outer segment structure influences the apparent kinetic parameters of cyclic GMP phosphodiesterase. *J Gen Physiol*. 1994;103:1071–1098.
8. Leskov IB, Klenchin VA, Handy JW, et al. The gain of rod phototransduction: reconciliation of biochemical and electrophysiological measurements. *Neuron*. 2000;27:525–537.
9. Fesenko EE, Kolesnikov SS, Lyubarsky AL. Induction by cyclic GMP of cationic conductance in plasma membrane of retinal rod outer segment. *Nature*. 1985;313:310–313.
10. Kaupp UB, Seifert R. Cyclic nucleotide-gated ion channels. *Physiol Rev*. 2002;82:769–824.
11. Pugh EN Jr, Lamb TD. Chapter 5 Phototransduction in vertebrate rods and cones: molecular mechanisms of amplification, recovery and light adaptation. *Handbook of Biological Physics*. 2000;3:183–255.
12. Forti S, Menini A, Rispoli G, Torre V. Kinetics of phototransduction in retinal rods of the newt Triturus cristatus. *J Physiol*. 1989;419:265–295.
13. Hartong DT, Berson EL, Dryja TP. Retinitis pigmentosa. *Lancet*. 2006;368:1795–1809.
14. Daiger SP, Sullivan LS, Bowne SJ. Genes and mutations causing retinitis pigmentosa. *Clin Genet*. 2013;84:132–141.
15. Sohocki MM, Daiger SP, Bowne SJ, et al. Prevalence of mutations causing retinitis pigmentosa and other inherited retinopathies. *Hum Mutat*. 2001;17:42–51.
16. Tam BM, Moritz OL. Dark rearing rescues P23H rhodopsin-induced retinal degeneration in a transgenic Xenopus laevis model of retinitis pigmentosa: a chromophore-dependent mechanism characterized by production of N-terminally truncated mutant rhodopsin. *J Neurosci*. 2007;27:9043–9053.
17. Lee DC, Vazquez-Chona FR, Ferrell WD, et al. Dysmorphic photoreceptors in a P23H mutant rhodopsin model of retinitis pigmentosa are metabolically active and capable of regenerating to reverse retinal degeneration. *J Neurosci*. 2012;32:2121–2128.
18. Bogéa TH, Wen RH, Moritz OL. Light induces ultrastructural changes in rod outer and inner segments, including autophagy, in a transgenic Xenopus laevis P23H rhodopsin model of retinitis pigmentosa autophagy in P23H light-induced retinal degeneration. *Invest Ophthalmol Vis Sci*. 2015;56:7947–7955.
19. Tam BM, Moritz OL. Characterization of rhodopsin P23H-induced retinal degeneration in a Xenopus laevis model of retinitis pigmentosa. *Invest Ophthalmol Vis Sci*. 2006;47:3234–3241.
20. Haeri M, Knox BE. Rhodopsin mutant P23H destabilizes rod photoreceptor disk membranes. *PLoS One*. 2012;7:e30101.
21. Sung CH, Davenport CM, Hennessey JC, et al. Rhodopsin mutations in autosomal dominant retinitis pigmentosa. *Proc Natl Acad Sci U S A*. 1991;88:6481–6485.
22. Paskowitz DM, Lavail MM, Duncan JL. Light and inherited retinal degeneration. *Br J Ophthalmol*. 2006;90:1060–1066.
23. Ramon E, Cordomí A, Aguilà M, et al. Differential light-induced responses in sectorial inherited retinal degeneration. *J Biol Chem*. 2014;289:35918–35928.

24. Noorwez SM, Malhotra R, McDowell JH, Smith KA, Krebs MP, Kaushal S. Retinoids assist the cellular folding of the autosomal dominant retinitis pigmentosa opsin mutant P23H. *J Biol Chem*. 2004;279:16278–16284.
25. Kaushal S, Khorana HG. Structure and function in rhodopsin. 7. Point mutations associated with autosomal dominant retinitis pigmentosa. *Biochemistry*. 1994;33:6121–6128.
26. Tam BM, Qazalbash A, Lee HC, Moritz OL. The dependence of retinal degeneration caused by the rhodopsin P23H mutation on light exposure and vitamin a deprivation. *Invest Ophthalmol Vis Sci*. 2010;51:1327–1334.
27. Chen Y, Jastrzebska B, Cao P, et al. Inherent instability of the retinitis pigmentosa P23H mutant opsin. *J Biol Chem*. 2014; 289:9288–9303.
28. Sakami S, Kolesnikov AV, Kefalov VJ, Palczewski K. P23H opsin knock-in mice reveal a novel step in retinal rod disc morphogenesis. *Hum Mol Genet*. 2014;23:1723–1741.
29. Sakami S, Maeda T, Bereta G, et al. Probing mechanisms of photoreceptor degeneration in a new mouse model of the common form of autosomal dominant retinitis pigmentosa due to P23H opsin mutations. *J Biol Chem*. 2011;286:10551–10567.
30. Tam BM, Noorwez SM, Kaushal S, Kono M, Moritz OL. Photoactivation-induced instability of rhodopsin mutants T4K and T17M in rod outer segments underlies retinal degeneration in X. laevis transgenic models of retinitis pigmentosa. *J Neurosci*. 2014;34:13336–13348.
31. Mazzolini M, Facchetti G, Andolfi L, et al. The phototransduction machinery in the rod outer segment has a strong efficacy gradient. *Proc Natl Acad Sci U S A*. 2015;112: E2715–E2724.
32. De Palo G, Facchetti G, Mazzolini M, Menini A, Torre V, Altafini C. Common dynamical features of sensory adaptation in photoreceptors and olfactory sensory neurons. *Sci Rep*. 2013;3:1251.
33. Rieke F, Baylor DA. Origin of reproducibility in the responses of retinal rods to single photons. *Biophys J*. 1998;75:1836–1857.
34. Lamb TD, McNaughton PA, Yau KW. Spatial spread of activation and background desensitization in toad rod outer segments. *J Physiol*. 1981;319:463–496.
35. Vent-Schmidt RYJ, Wen RH, Zong Z, et al. Opposing effects of valproic acid treatment mediated by histone deacetylase inhibitor activity in four transgenic X. laevis models of retinitis pigmentosa. *J Neurosci*. 2017;37:1039–1054.
36. Schindelin J, Rueden CT, Hiner MC, Eliceiri KW. The ImageJ ecosystem: an open platform for biomedical image analysis. *Mol Reprod Dev*. 2015;82:518–529.
37. Xiong W-H, Yau K-W. Rod sensitivity during Xenopus development. *J Gen Physiol*. 2002;120:817–827.
38. Solessio E, Mani SS, Cuenca N, Engbretson GA, Barlow RB, Knox BE. Developmental regulation of calcium-dependent feedback in Xenopus rods. *J Gen Physiol*. 2004;124:569–585.
39. Matthews HR, Fain GL, Murphy RL, Lamb TD. Light adaptation in cone photoreceptors of the salamander: a role for cytoplasmic calcium. *J Physiol*. 1990;420:447–469.
40. Lobanova ES, Herrmann R, Finkelstein S, et al. Mechanistic basis for the failure of cone transducin to translocate: why cones are never blinded by light. *J Neurosci*. 2010;30:6815–6824.
41. Lobanova ES, Finkelstein S, Song H, et al. Transducin translocation in rods is triggered by saturation of the GTPase-activating complex. *J Neurosci*. 2007;27:1151–1160.
42. Gunkel M, Schöneberg J, Alkhaldi W, et al. Higher-order architecture of rhodopsin in intact photoreceptors and its implication for phototransduction kinetics. *Structure*. 2015; 23:628–638.
43. Liang Y, Fotiadis D, Filipek S, Saperstein DA, Palczewski K, Engel A. Organization of the G protein-coupled receptors rhodopsin and opsin in native membranes. *J Biol Chem*. 2003;278:21655–21662.
44. Fotiadis D, Liang Y, Filipek S, Saperstein DA, Engel A, Palczewski K. Atomic-force microscopy: rhodopsin dimers in native disc membranes. *Nature*. 2003;421:127–128.
45. Liang Y, Fotiadis D, Maeda T, et al. Rhodopsin signaling and organization in heterozygote rhodopsin knockout mice. *J Biol Chem*. 2004;279:48189–48196.
46. Govardovskii VI, Korenyak DA, Shukolyukov SA, Zueva L V. Lateral diffusion of rhodopsin in photoreceptor membrane: a reappraisal. *Mol Vis*. 2009;15:1717–1729.
47. Palczewski K, Kumasaka T, Hori T, et al. Crystal structure of rhodopsin: a G protein-coupled receptor. *Science*. 2000;289: 739–745.
48. Kraft TW, Allen D, Petters RM, Hao Y, Peng Y-W, Wong F. Altered light responses of single rod photoreceptors in transgenic pigs expressing P347L or P347S rhodopsin. *Mol Vis*. 2005;11:1246–1256.
49. Makino CL, Wen X-H, Michaud NA, et al. Rhodopsin expression level affects rod outer segment morphology and photoresponse kinetics. *PLoS One*. 2012;7:e37832.
50. Tam BM, Moritz OL. The role of rhodopsin glycosylation in protein folding, trafficking, and light-sensitive retinal degeneration. *J Neurosci*. 2009;29:15145–15154.
51. Moritz OL, Tam BM. Recent insights into the mechanisms underlying light-dependent retinal degeneration from X. laevis models of retinitis pigmentosa. *Adv Exp Med Biol*. 2010;664:509–515.
52. Moritz OL, Tam BM. Recent insights into the mechanisms underlying light-dependent retinal degeneration from x. Laevis models of retinitis pigmentosa. *Adv Exp Med Biol*. 2010;664:509–515.
53. Price BA, Sandoval IM, Chan F, et al. Mislocalization and degradation of human P23H-rhodopsin-GFP in a knockin mouse model of retinitis pigmentosa. *Invest Ophthalmol Vis Sci*. 2011;52:9728–9736.
54. Illing ME, Rajan RS, Bence NF, Kopito RR. A rhodopsin mutant linked to autosomal dominant retinitis pigmentosa is prone to aggregate and interacts with the ubiquitin proteasome system. *J Biol Chem*. 2002;277:34150–34160.
55. Athanasiou D, Aguila M, Bellingham J, et al. The molecular and cellular basis of rhodopsin retinitis pigmentosa reveals potential strategies for therapy. *Prog Retin Eye Res*. 2018; 62:1–23.
56. Athanasiou D, Aguila M, Opefit CA, et al. Rescue of mutant rhodopsin traffic by metformin-induced AMPK activation accelerates photoreceptor degeneration. *Hum Mol Genet*. 2017;26:305–319.
57. Kemp CM, Jacobson SG, Roman AJ, Sung CH, Nathans J. Abnormal rod dark adaptation in autosomal dominant retinitis pigmentosa with proline-23-histidine rhodopsin mutation. *Am J Ophthalmol*. 1992;113:165–74.
58. Moore A, Fitzke FW, Kemp CM, et al. Abnormal dark-adaptation kinetics in autosomal dominant sector retinitis-pigmentosa due to rod opsin mutation. *Br J Ophthalmol*. 1992;76:465–469.
59. Goto Y, Peachey NS, Ripps H, Naash MI. Functional abnormalities in transgenic mice expressing a mutant rhodopsin gene. *Invest Ophthalmol Vis Sci*. 1995;36:62–71.

Investigative Ophthalmology & Visual Science